An Interdisciplinary Approach to Local Strength Assessment of Cast Iron Components to Exploit Unused Component Potential

Felix Weber, Vitali Züch, Christian Gebhardt, Alexander Bezold, Christoph Broeckmann, Dennis Bosse, Georg Jacobs, Vitalii Gurevich, Mathias Bodenburg

Abstract:
Modern cast iron components used for structural applications in wind turbines are continuously growing in size due to the rising demand for renewable energy. With current power-to-weight ratios of up to 20 tons of cast iron per megawatt, interdisciplinary approaches must be applied to increase the local component utilization and successively reduce component weights in order to meet manufacturing and logistics challenges. Besides the demand for reduced component weights, interdisciplinary approaches are needed to enable new design methodologies for cast iron components to ensure manufacturability and castability.
The IEC 61400 standard and FKM guideline are common frameworks for the design of cast iron components for wind turbines. Usually, constant values for the tensile or fatigue strength are often applied to entire component regions to ensure sufficient component safety. However, large-volume cast iron components often exhibit enormous variations in local material properties due to different microstructures resulting from varying cooling conditions in the component. Utilizing the locally resolved material strength can open up access to unused component potential.
To determine the locally resolved material strength, an interdisciplinary approach based on casting simulation, micromechanical analysis, and local strength assessment is required. Based on casting simulation, local microstructure descriptors, such as particle count or size distribution of graphite precipitates, are determined across the component. Subsequent micromechanical analysis results in local material strength estimates for the entire component, which are used in the local strength assessment. To determine the component potential, micromechanical analysis and strength assessment are performed iteratively to cover the range of potential local microstructure states.
In this study, a torque arm of grade EN-GJS-500-14 used in a modern wind turbine gearbox is analyzed to demonstrate the potential of the proposed approach. Casting simulations of the torque arm are performed to determine the expected local microstructures and the risk of local shrinkage cavities. Using microstructure descriptors obtained from the casting simulation, the local microstructure is reconstructed and analyzed micromechanically, resulting in an estimate of the fatigue strength. Based on this estimation, optimization of the torque arm is performed with respect to the local strength assessment.

Keywords: Ductile Cast Iron, Fatigue Strength, Shakedown Analysis, Strength Assessment, Shape Optimization

1 Introduction

Modern wind energy turbines play an essential role within the transition towards the declared goal of a carbon neutral society [1]. To achieve these goals, the total power installed of wind turbines and especially the individual power per wind turbine are increasing. Considering that up to 20 metric tons of cast iron are used per installed megawatt, better utilization of the material could result in considerable weight reduction. Heavy-section castings, such as the main shaft or torque arm, which are typically subjected to cyclic loading, are examples of these major components [2]. Due to the increasing weight of cast iron components, logistical and manufacturing challenges arise. To overcome these challenges, an increase in the power-to-weight ratio is required.

Until now, the power-to-weight ratio of heavy-section castings has generally been limited by the strength assessment. In common concepts of strength assessment, such as FKM guideline, safety factors lead to a significant reduction of local material properties [3]. As a solution, approaches have been developed to directly consider local material properties in component design and to determine them efficiently:

First, the consideration of local material properties, such as the fatigue strength, has not been common practice for cast iron components in wind turbines. However, it has already been shown by Cenni [4] that considering local material properties in the component design of heavy-section castings is cost-effective. Several approaches to consider local material parameters in the strength assessment of casted components have been developed: Olofsson et al. presented a multidisciplinary approach based on the determination of local material parameters determined by experimental correlations and numerical analysis of representative volume elements (RVE) [5–7]. However, this approach relies on the prediction of local solidification behavior so that local solidification models for heavy-section castings are established [8]. Subsequently, direct correlations between casting simulation and microstructure dependent material properties, such as fatigue strength, were made [9]. Besides the structural analysis, an increase in component potential by optimization of local cooling conditions was identified by Dobrovska et al. [10].

Second, for ductile cast iron, several microstructure-based modeling approaches are known and commonly used to determine microstructure-sensitive strenghts with less effort than experimental testing. Based on unit-cell models, Bonora [11] modeled the damage mechanisms around graphite in ferritic ductile cast iron. To account for complex material models, Andriollo considered anisotropy and plasticity [12,13]. Combining micromechanical simulation with strain-based measurements, Andriollo and Gebhardt [14,15] apply a calibration of material parameters, especially of the matrix, to ductile cast iron. Combining the results of these approaches in the context of a shakedown analysis, Gebhardt was able to estimate the fatigue strength of ductile cast iron [16,17]. However, in contrast to simulation-based approaches, microstructure-property relations for ferritic ductile cast iron have been established by Donelan [18] to estimate the ultimate tensile strength and yield strength based on microstructure parameters.

In conclusion, a combination of fatigue strength prediction and modified strength assessment for heavy-section castings in wind turbines has not yet been established. Thus, modern wind turbines miss out on a significant potential for weight reduction.

This study presents an approach to consider a local strength assessment in the design of heavy-section castings, demonstrated using the torque arm, made of cast iron grade EN-GJS-500-14, of a 3 MW research nacelle. To determine the potential for weight reduction, material characterization and experimental fatigue testing were performed. Based on the correlation of microstructure and experimental testing, microstructure-property relationships are determined. Furthermore, the fatigue strength is estimated using simulation-based shakedown analysis of the microstructure. In combination with the casting simulation, this allows for a high resolution of local fatigue strength within the casting component. Subsequently, the local fatigue strength is considered in a modified strength assessment of a wind turbine gearbox torque arm, which is used as a demonstrator component. Finally, the weight reduction potential of the torque arm is estimated based on a shape optimization considering the results of the local strength assessment.

2 Material

The heavy-section casting investigated in this study is a ferritic ductile cast iron of grade EN-GJS-500-14. Sampling was done based on cubes of edge lengths of 200, 300, and 500 mm (casting modules 3.3, 5.0, and 8.3 cm, respectively) cast in a sand mold by foundry Silbitz Group Torgelow. Material characterization was performed using specimens from the center of each cube, while fatigue testing was performed using samples from the entire cubes. The microstructure descriptors, analyzed accordingly to standard EN 945-4 [19] using five micrographs of size 1.387 x 1.045 mm in 100x magnification, are given in Tab. 1.

Tab. 1 Microstructure descriptors according to EN 945-4 for different casting modules.

Casting Modulus	3.3 cm	5.0 cm	8.3 cm
Graphite Phase Fraction [%]	10.5	13.8	13.5
max. Feret Diameter [µm]	118.8	140.2	187.6
Nodularity [-]	0.846	0.821	0.769
Particle Count [1/mm2]	91.6	84.2	46.8

Tab. 2 Chemical analysis of the investigated grade EN-GJS-500-14.

Element	wt.-%	Element	wt.-%
C	3.41	S	<0.01
Si	3.22	Mg	<0.05
Mn	0.20	Fe	bal.
P	<0.02		

Tab. 3 Results of quasi-static mechanical testing.

Casting Modulus	3.3 cm	5.0 cm	8.3 cm
Ultimate Tensile Strength [MPa]	473	466	454
Yield Strength [MPa]	348	345	339
Fracture Elongation [%]	20	18	14

Chemical analysis was performed by optical emission spectroscopy (OES), the results are given in Tab. 2. The static mechanical properties were determined in uniaxial tensile tests using five type A specimens of diameter 8 mm according to DIN 50125 [20]. Results are summarized in Tab. 3.

3 Methodology

This study presents an optimization approach for heavy-section castings based on casting simulation, micromechanical analysis, strength assessment, and subsequent shape optimization, as shown in Fig. 1.

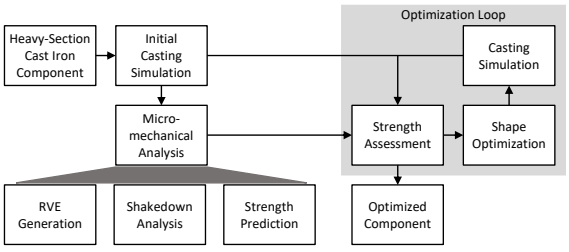


Fig. 1 Overview of the presented component optimization scheme.

Based on an initial casting simulation, representative regions of the local solidification behavior are selected for further micromechanical analysis. Here, the micromechanical analysis comprises RVE generation, shakedown analysis, and subsequent strength prediction. These results are validated against prior experimental testing. Using the predicted material strength in a modified strength assessment, shape optimization is iteratively performed in combination with a casting simulation until the component reaches its optimization limits within the allowable geometric limits.

3.1 Fatigue Testing

Load-controlled fatigue tests were performed using the specimen geometry shown in Fig. 2.

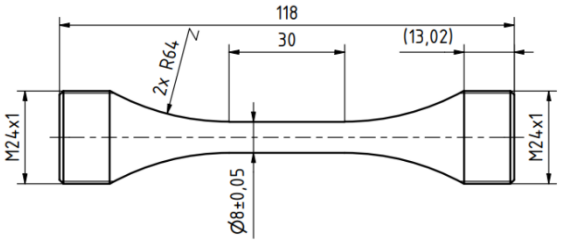


Fig. 2 Specimen geometry used for uniaxial fatigue testing.

The specimens were subjected to uniaxial loading with a stress ratio of $R = -1$ and testing frequencies of around 112 Hz. Testing was performed by the stair-step method with a Roell Amsler high-frequency pulsator (type HFP 422) according to DIN 50100 [21] with a logarithmic increment of $d_{log} = 1.069$. Remaining specimens and runouts were used to determine the finite life regime. Results were analysed using the software SAFD 5 (Statistical Analysis of Fatigue Data) [22].

3.2 Shakedown Analysis

A material subject to cyclic loading can exhibit different stress-strain patterns, as shown in Fig. 3.

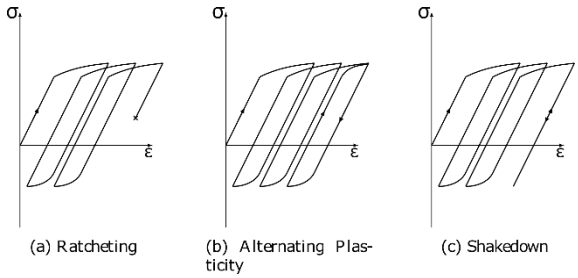


Fig. 3 Material response for cyclic loading patterns.

The shown stress-strain patterns of alternating plasticity and ratcheting lead to failure of the material. In contrast, the shakedown state is characterized by a purely elastic deformation after a finite number of initial loading cycles with plastic deformation. Thus, a material in a shakedown state will not fail due to fatigue. For composite materials, the shakedown

state was investigated by Weichert et al. [23]. Accordingly to [23], the shakedown state is governed by the development of a time-invariant residual stress field $\bar{\rho}$ in the material's microstructure. The residual stress field develops due to the accumulation of local plasticity in the very first loading cycles and is superimposed on the purely elastic stress field σ^e caused by external loading [23]. Thus, the locally acting stress is defined by

$$\sigma = \sigma^e + \bar{\rho}$$

Once reaching a shakedown state, which is indicated by a purely linear elastic material response, the plastic dissipation is bounded such that no further plastic strain occurs in the microstructure [24].

Determination of the shakedown state can be achieved by evaluation of the static theorem for shakedown, as formulated by Melan [25]:

> *If there exists a factor* $\lambda > 1$ *and a time-independent residual stress field* $\bar{\rho}$ *with*
> $\int_V \bar{\rho} : \mathbb{D} : \bar{\rho} dV < \infty$,
> *with compliance tensor* $\mathbb{D}$ *, such that for all loads* **B** *in the load domain the following inequality is satisfied*
> $f(\lambda\sigma^e + \bar{\rho}) \leq 0$,
> *then the structure will shake down under the given load domain.*

Here, f is a yield criterion, e.g. the von Mises yield criterion. For complex geometries, such as microstructures, evaluation of this state must be performed numerically. Thus, Chen [24] implemented the FEM-based evaluation applied here, which results in the maximum admissible residual stress field under a given loading by solving the following optimization problem:

$$\begin{aligned} &maximize && \lambda \\ &subject\ to && \nabla \cdot \bar{\rho} = 0\ in\ \Omega \\ & && \bar{\rho} \cdot n = 0\ on\ \Gamma \\ &f(\lambda\sigma_k^e + \bar{\rho}_k) \leq \sigma_Y^2 && k = 1, .., NV \end{aligned}$$

Here, NV represents the number of load vertices that define the load domain. Solving this optimization problem results in the maximal load (fatigue load) to which the material may be subjected without suffering damage.

3.3 RVE Generation

Representative Volume Elements (RVE) used for the numerical analysis of the given local cast iron microstructures define a domain that is sufficiently large to represent the characteristics of a microstructure under analysis. Here, RVEs represent the microstructure consisting of a ferrite matrix with graphite precipitates. Based on the RVE, a computational domain can be constructed that can be used in finite element analysis (FEA), for example, to predict fatigue strength.

In general, the RVE used for FEA analysis can be constructed based on real micrographs or artificially reconstructed using characteristic microstructure descriptors [17]. In the case of RVE based on micrographs, the graphite precipitates and smaller shrinkages are identified by applying thresholds during image analysis. Subsequently, these are embedded in the ferritic matrix (comp. Fig. 4).

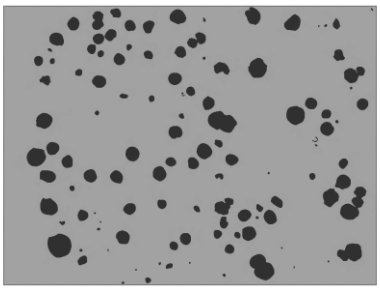


Fig. 4 Exemplary RVE with graphite precipitates (dark) and ferrite matrix (bright).

Artificial RVEs are reconstructed in this case based on the Gumbel distribution, which describes the size distribution (max. feret diameter) of graphite precipitates and is obtained by digital image analysis. Using a database of real defect contours of various sizes, a random sequential adsorption [26] (RSA) based algorithm places graphite precipitates in the computational domain until the predefined size distribution and phase fraction are reached. Fig. 5 gives a visual comparison of RVE based on micrographs and artificial RVE.

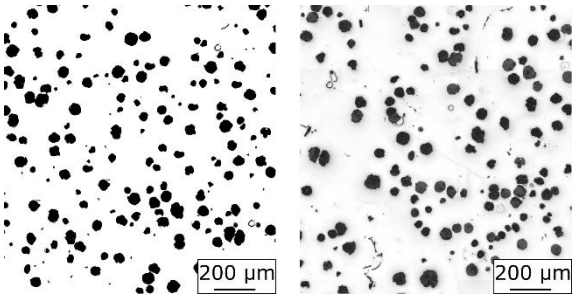


Fig. 5 Artificial RVE (left) compared to a real micrograph (right).

For subsequent mechanical analysis, the RVEs are converted into a 2.5D model (by extrusion in the third dimension) to avoid pure plane stress or plane strain states.

3.4 Casting Simulation

Within the presented optimization approach, the casting simulation is used to predict the local solidification behavior. The classical approach to predict the solidification times of castings or their particular sections is to use the modulus (casting modulus). This modulus M is defined by the ratio of the volume V and the surface (cooling surface) S of the casting or a particular section

$M = V/S$

According to Chvorinov's rule [27], the local solidification time t_S is proportional to the square of the modulus

$t_S = \mathrm{c} \cdot M^2$

with c as a constant depending amongst others on the cast alloy, the mold material, and the pouring temperature.

This "classical" modulus is a parameter solely depending on geometrical dimensions not taking into consideration that during the cooling of a casting the heat flow conditions are transient. Neighboring parts or sections in a mold or auxiliary materials like cooling chills or insulating sleeves will influence the cooling behavior.

For this reason, in up-to-date foundry process simulation tools the thermal modulus (or feeding modulus/feedmod) usually is used. This feedmod is calculated based on the simulated solidification time and, therefore, much more accurate than its geometrical counterpart.

Often feedmod and local solidification time are used synonymously, whereas feedmod usually gives a better sense of solidification behavior and necessary measures to take because data sheets of feeders used to achieve pore-free castings contain this information.

Moreover, many characteristics, e.g. ferrite grain size, are depending on the local solidification time and, as feedmod and local solidification time are interdependent, can be described by the feedmod as well.

3.5 Strength Assessment

One possible approach for the strength assessment of cast iron components is given by the FKM guideline. For a strength assessment according to FKM, the critical component region, which is the potential region of crack initiation, is analyzed in detail. The procedure required for the strength assessment under static and cyclic loading is presented in Fig. 6.

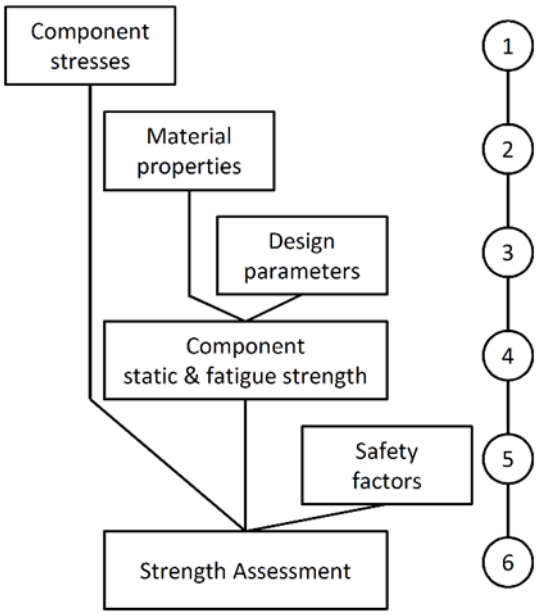


Fig. 6 Procedure of calculation for an assessment of the static and fatigue strength, based on FKM guideline [3].

As shown in Fig. 6, the strength assessment consists of several steps: First, the stress within the component, the material strength according to standards, and the component design parameters are determined. Subsequently, the component strength is determined and the degree of utilization is calculated considering the required safety factors [3]. Here, a local strength assessment can be enforced by strictly considering the estimated local material parameters such that the local heterogeneity of cast iron is taken care of.

According to FKM, the utilization a is defined by the ratio of the component stress and the component strength reduced by the required safety factor:

$$a = \frac{\sigma}{\sigma_{all}/\mathrm{j}}$$

with the apparent stress σ and allowable stress (for a 2.5 % failure probability) σ_{all} as well as safety factor j. With respect to local material properties, especially the safety factor as well as the allowable stress are of interest. Due to the high heterogeneity of cast iron materials, cast iron specific safety factors of 1.25 to 1.4 are considered. The allowable stress in terms of fatigue strength for a load ratio of $R = -1$ is for the given cast iron grade estimated by

$$\sigma_{WK} = \sigma_{W,zd}/K_{WK,\sigma}$$

$$\sigma_{W,zd} = f_{W,\sigma} \cdot R_m = (0.25 + \frac{70\ MPa}{R_{m,N}}) \cdot R_m$$

Here, $K_{WK,\sigma}$ is a component specific design parameter and R_m is governed by the tensile strength $R_{m,N}$ according to standards such that

$$R_m = K_{d,m} \cdot R_{m,N}$$

with $K_{d,m}$ being the technological size factor. The technological size factor $K_{d,m}$ depends on the component's effective diameter such that for complex 3D geometries an estimation based on Volume V and surface S is suggested

$$d_{eff} = \frac{4 \cdot V}{S}$$

Thus, geometric influences and material heterogeneity are considered based on the technological size factor $K_{d,m}$ and safety factor j.

In order to reduce the influence of said factors, the presented local strength assessment considers estimated local material properties such as the tensile strength R_m or yield strength R_p and fatigue strength $\sigma_{W,zd}$, which can be directly used in the given strength assessment. As the heterogeneity of the investigated material is considered during the estimation of local material properties a further reduction of safety factors may open up additional design freedom.

4 Results and Discussion

4.1 Fatigue Testing

Results of the load-controlled fatigue tests with $R = -1$ for the three investigated casting modules are presented in Fig. 7, Fig. 8, and Fig. 9.

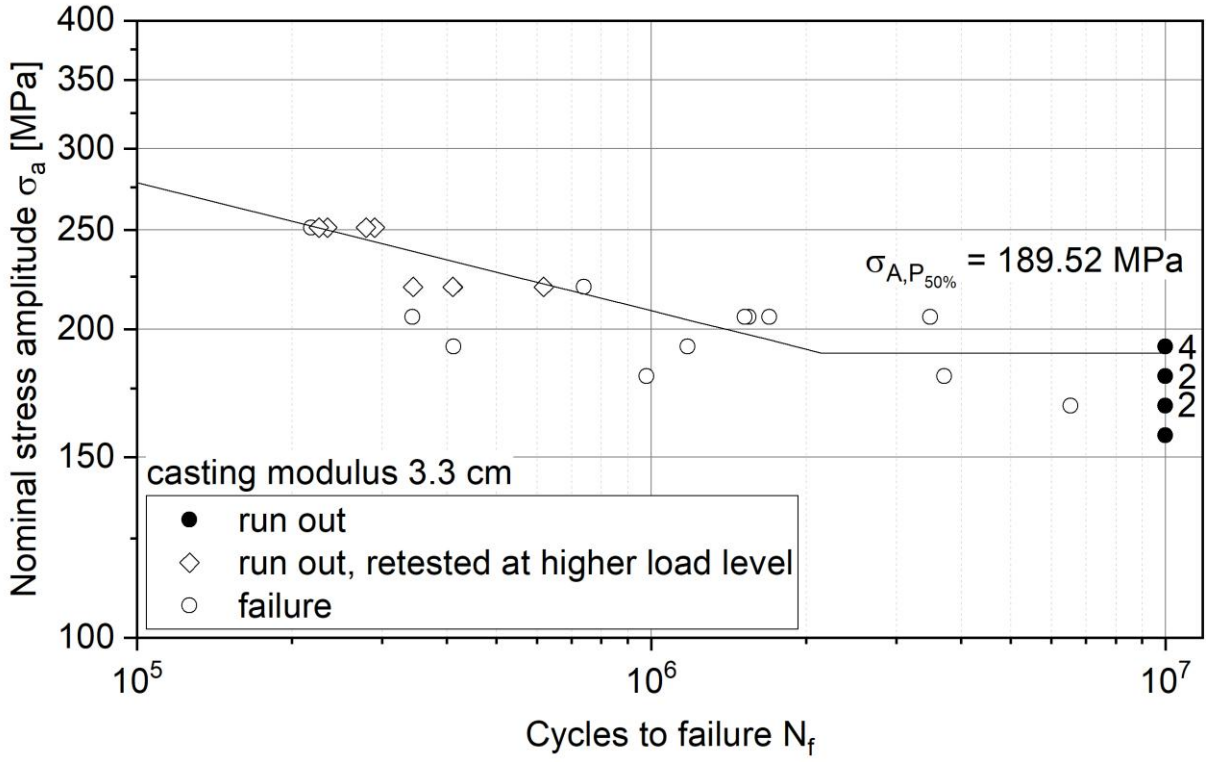


Fig. 7 Results of fatigue testing for casting modulus 3.3 cm.

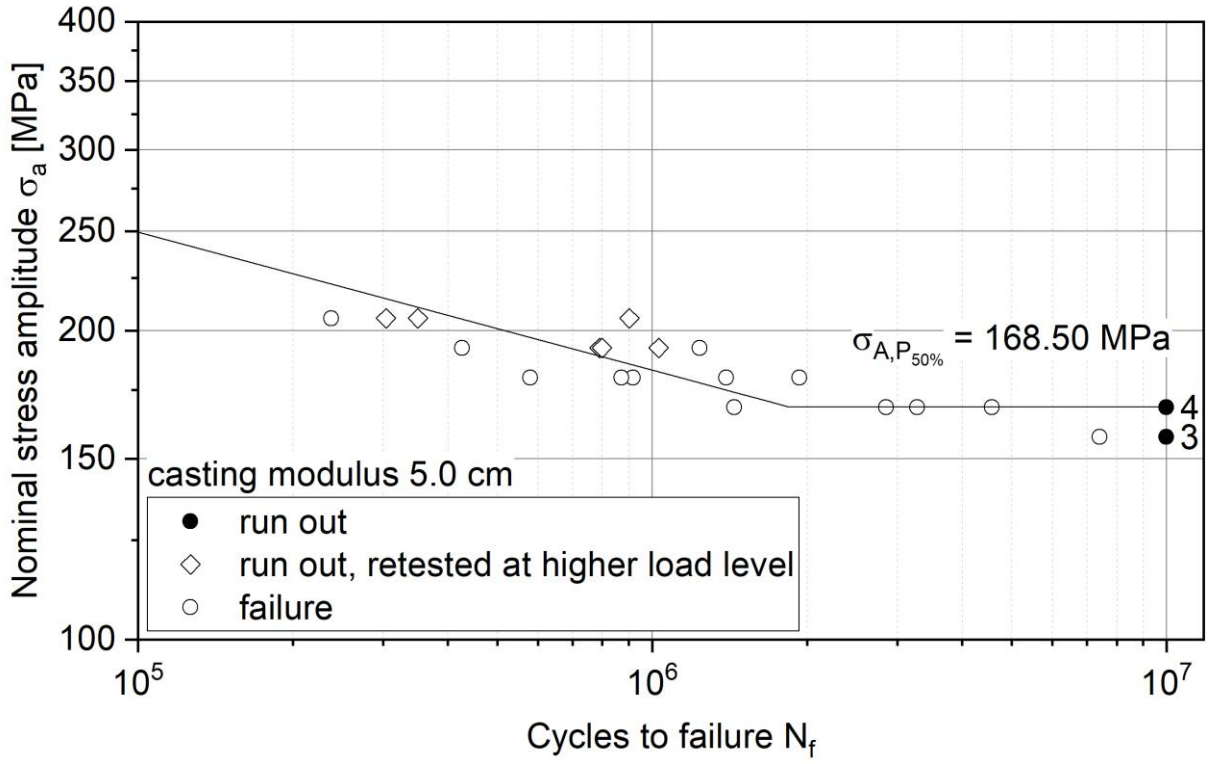


Fig. 8 Results of fatigue testing for casting modulus 5.0 cm.

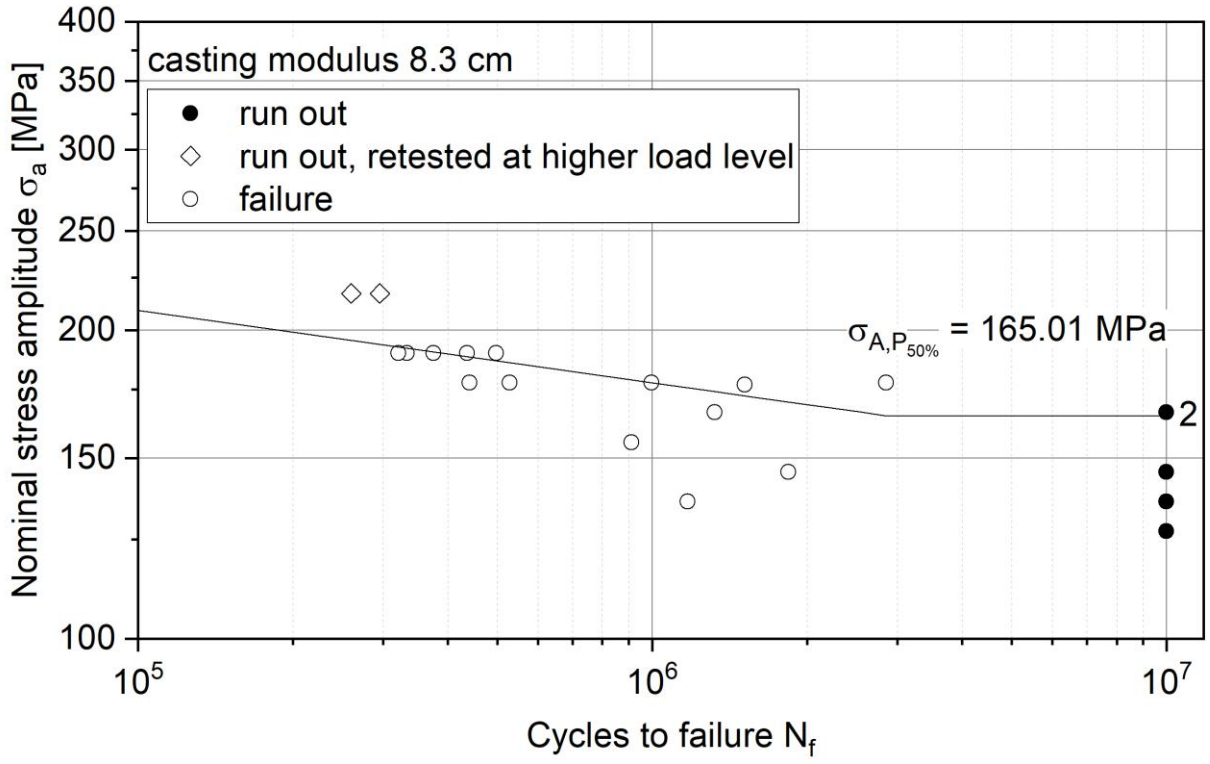


Fig. 9 Results of fatigue testing for casting modulus 8.3 cm.

The casting modulus of 3.3 cm presents the best fatigue strength with $\sigma_{A,P_{50\%}} = 189.5\ MPa$ and a scatter band $T_\sigma = 1.344$, with $T_\sigma = \frac{\sigma_{A,P_{90\%}}}{\sigma_{A,P_{10\%}}}$. For the casting modules 5.0 cm and 8.3 cm $\sigma_{A,P_{50\%}} = 165\ MPa$ with $T_\sigma = 1.171$ and $\sigma_{A,P_{50\%}} = 168.5 MPa$ with $T_\sigma = 1.315$ can be observed, respectively. Thus, an increasing casting modulus results in a reduced fatigue strength. The fatigue strengths for a 2.5 % failure probability $\sigma_{A,P_{2,5\%}}$ required by conventional strength assessments, such as FKM, are computed using the probability measures determined from the results of experimental fatigue testing and are given in Tab. 4.

Tab. 4 Fatigue strengths for tested casting modules determined by SAFD 5.

Casting Modulus [cm]	$\sigma_{A,P_{2.5\%}}$ [MPa]	$\sigma_{A,P_{50\%}}$ [MPa]
3.3 cm	146.8 MPa	189.5 MPa
5 cm	148.1 MPa	168.5 MPa
8.3 cm	130.6 MPa	165 MPa

SEM-analysis of the fracture surfaces of cracked specimens allowed for evaluation of the size of crack initiating defects. Here, the size is measured as the projected area of the defect normal to the loading direction.

As can be seen in Fig. 10, the defect size increases with increasing casting modulus. Furthermore, based on the analysis of 36 fracture surfaces, only two specimens showed crack initiation at a graphite precipitate. For the remaining 34 fracture surfaces, shrinkages could be identified as crack initiation sides, which is in accordance with [28] for heavy-section ductile cast iron.

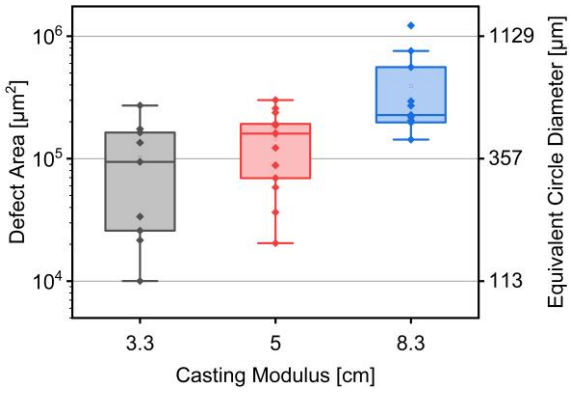


Fig. 10 Defect size distribution on fracture surface among experimentally tested casting modulus.

Comparison of the experimentally determined S-N-curves with synthetic S-N-curves governed by FKM, as shown in Fig. 11, reveals an overestimation of the fatigue strength by FKM by 26%. This can be associated with the porosity observed within the tested material. Borgs [29] analyzed that the effect of porosity in ductile cast iron is more dominant on the fatigue strength than on its tensile strength. Since the S-N curve governed by FKM is based on the material's tensile strength, it does not account for the given porosity in contrast to the experimentally determined S-N curve and is subsequently corrected using the cast iron specific safety factor.

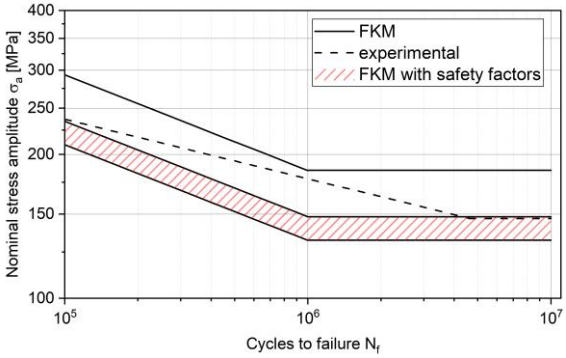


Fig. 11 Comparison of S-N curves estimated by FKM and experimentally for casting modulus 3.3 cm.

4.2 Microstructure-Property Relationships

Casting simulations were performed using MAGMAsoft in order to obtain local cooling conditions and microstructure estimations for each casted cube. Here, the casting system of the cubes has been remodeled in MAGMAsoft considering casting in sand without further modifications.

Combining the results of the casting simulation with the known specimen layout, 18 tested fatigue specimens (6 per cube size) with individual feedmods between 2.24 and 8.56 cm were selected for further metallographic analysis. Each specimen was cut close to the fracture surface and a microsection has been prepared by polishing as well as etching (Nital 3%, 30 sec). Micrographs were obtained using an optical light microscope. By applying digital image analysis using FIJI [30], the graphite fraction [%], graphite nodularity [-], particle count [1/mm^2], and max. feret diameter [µm] were analyzed. Here, a minimum size of 10 µm is used as a lower diameter threshold for graphite precipitates to be considered. The results of the analysis with respect to the simulated feedmod are shown in Fig. 12 and Fig. 13.

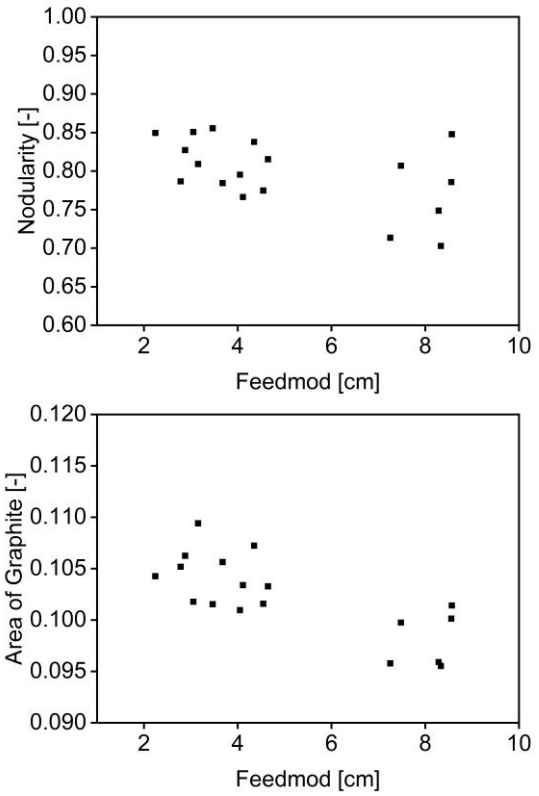


Fig. 12 Correlation of nodularity and graphite area with simulative feedmod.

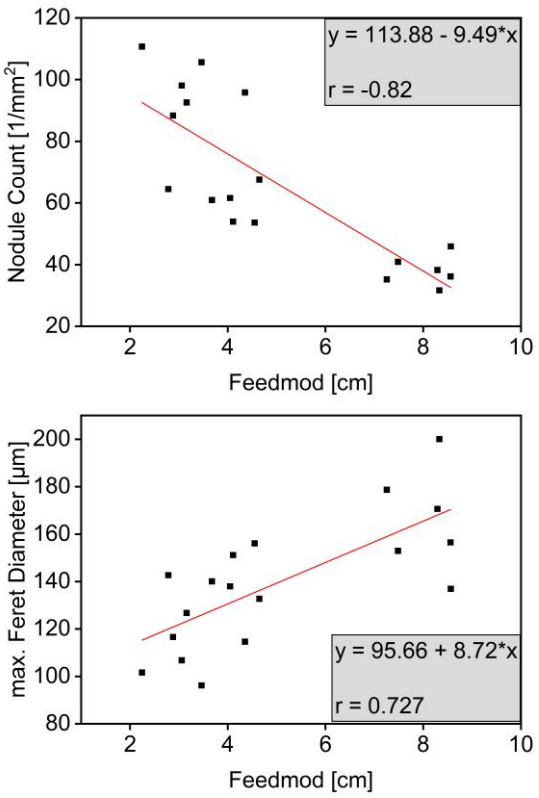


Fig. 13 Correlation of nodule count and max. feret diameter with simulative feedmod (linear fit with corresponding Pearson correlation coefficient).

Here, the graphite fraction and nodularity are only slightly affected by the feedmod. The observed decrease in nodularity may be related to graphite degeneration due to elongated solidification and cooling times. The variation within the graphite fraction is in a range associable with artifacts due to automated digital image analysis, such that it is considered to be neglectable. The increase of the max. feret diameter as well as the decrease of the particle count are related to the increasing size of individual graphite precipitates with elongated cooling.

Using the line interception method, the average ferrite grain size was estimated. As shown in Fig. 14, the ferrite grain size increases with the max. feret diameter as well as the feedmod.

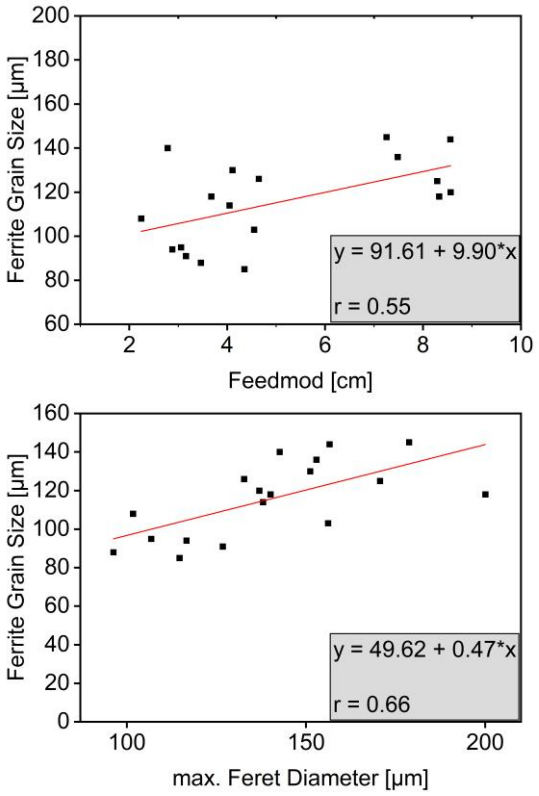


Fig. 14 Correlation of simulative feedmod and max. feret diameter with ferrite grain size (linear fit with corresponding Pearson correlation coefficient).

These correlations can be associated with the microstructure evolution during solidification and cooling: Graphite precipitates nucleate during solidification and form an enveloping austenite grain [31]. Subsequently, during cooling the austenite grain transforms into individual ferrite grains [31]. Thus, the average ferrite grain size is governed by the average “inter graphite precipitate” distance (which limits the prior austenite grain size) and the cooling conditions (which controls the collapse of prior austenite grains). Using microstructure estimators obtainable

from metallographic and simulative analysis, the distance between graphite precipitates and cooling conditions can be described using the particle count n_{pc} and the cooling rate t_{cool}, respectively. For the investigated specimen this leads to a formulation of the ferrite grain size $d_{ferrite}$ in dependence of the cooling rate t_{cool} and the particle count n_{pc}:

$$d_{ferrite} = 132.99\mu m + 0.000197\frac{\mu m}{s} \cdot t_{cool} - 0.379\mu m \cdot mm^2 \cdot n_{pc}$$

Considering Donelan's [18] relation between the ferrite grain size and the yield strength for ductile cast iron, a Hall-Petch like equation can be used to determine the ultimate tensile strength as well as yield strength for the given material:

$$\sigma_{ys} = 250.9\ MPa + \frac{1010\ MPa\sqrt{\mu m}}{\sqrt{d_{ferrite}}}$$

$$\sigma_{uts} = 266.5\ MPa + \frac{2144\ MPa\sqrt{\mu m}}{\sqrt{d_{ferrite}}}$$

both visualized in Fig. 15.

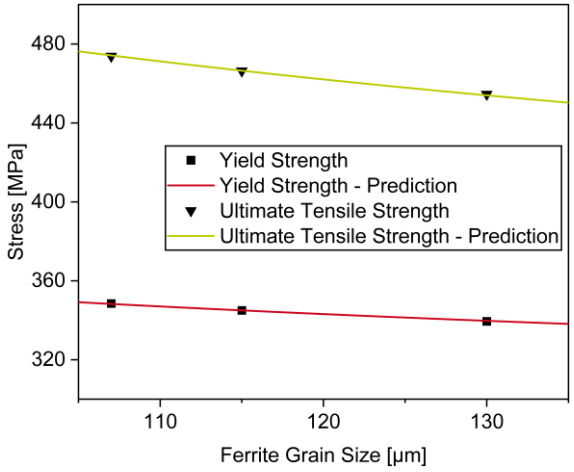


Fig. 15 Prediction of yield strength and ultimate tensile strength based on ferrite grain size (symbols indicate experimental test results).

4.3 Fatigue Strength Prediction

The efficiency of a local strength assessment scales directly with the resolution of known fatigue strengths. For the later strength assessment, the fatigue strength is required in dependence of the simulated feedmod. Thus, micrograph-based and artificial RVEs have been generated using the presented RVE generation approaches for feedmods which can be found in the critical regions during the strength assessment of the torque arm. As the phase fraction of graphite is nearly constant within the casting, only RVEs with a graphite phase fraction of 11.0 - 12.5 % have been used for shakedown analysis. Each RVE had a size of 1387 x 1045 x 10 µm.

Tab. 5 Material parameters used during shakedown analysis.

Material Property	Ferrite	Graphite
Young's Modulus [GPa]	210.63	32.21
Poisson Ratio [-]	0.3	0.25
Yield Strength [MPa]	461.2	150

Material parameters of ferrite and graphite used for shakedown analysis are given in Tab. 5. Both phases are considered to be elastic-perfectly plastic. Here, the yield strength of graphite is artificially increased to ensure the significance of the ferrite matrix, as experimentally observed, during shakedown. No debonding is considered at the interface of graphite precipitates and ferrite matrix. The fatigue strength has been computed for support points of the feedmod within the critical regions of the torque arm resulting in feedmods within the range of 2.7 cm to 4.7 cm. The computed shakedown limits are presented in Fig. 16. Here, the shakedown limit corresponds to the fatigue strength for a failure probability of 0 % at a stress ratio of $R = 0$, as the load vertices are $0\ N$ and the computed limited load. Due to high computational cost, the size of the RVE is limited which results in an increased scatter of the computed fatigue strengths. With increasing feedmod, the graphite precipitates grow in size and the particle count decreases such that the domain size of pure matrix or precipitate regions increases, especially in the size limited RVE used for shakedown analysis. Thus, the scatter width of shakedown results increases with the feedmod. Due to the size of the casting, the most critical RVEs need to be expected to be present in the actual component. Thus, the 10 % percentile fatigue strength is used to establish a conservative formulation for the feedmod dependent fatigue strength:

$$2\sigma_{a,P_{0\%}} = 249.4\ \mathrm{MPa} \cdot \mathrm{feedmod}^{-0.3352}$$

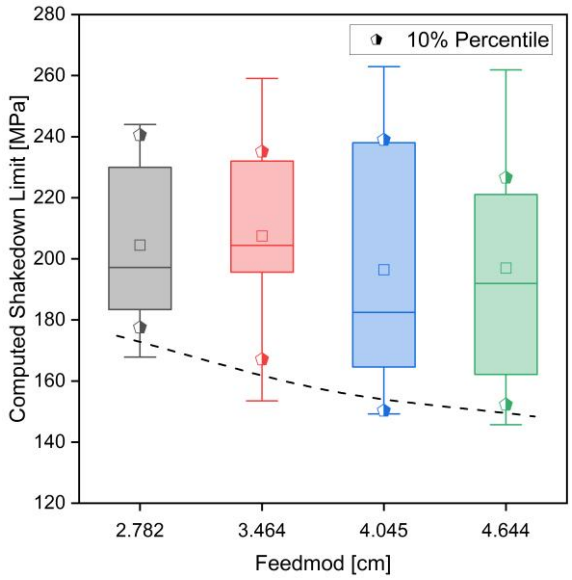


Fig. 16 Computed shakedown limit which equals $2\sigma_a$ for a stress ratio $R = 0$ with a fit (dashed line) through the lower 10 % percentile.

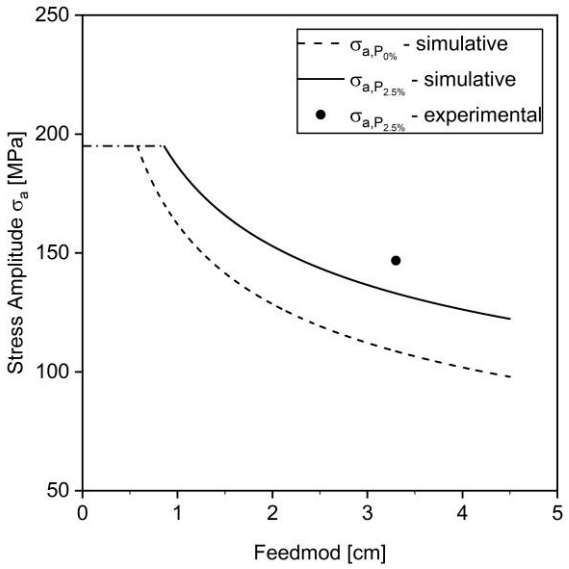


Fig. 17 Comparison of numerically computed shakedown limits vs. experimentally determined fatigue strength.

Transformation of the computed shakedown limit from $R = 0$ to $R = -1$ using the experimentally obtained Haigh-diagram for a casting modulus of 3.3 cm leads to

$$\sigma_{a,P_{0\%}} = 1.3 \cdot \frac{249.4\ \mathrm{MPa} \cdot \mathrm{feedmod}^{-0.3352}}{2}$$

Using the probability diagram based on the experimental fatigue testing of the 3.3 cm casting, the shakedown limit is increased by $24.37\ MPa$ for the increased failure probability of 2.5 %. The resulting curves of the numerical fatigue strength prediction are shown in Fig. 17. Here, a deviation of 10.4 % is still observed between numerical fatigue strength estimation and experimental results due to the conservative lower bound estimation of the shakedown theorem. This may be related to the disallowance of microstructural damage in shakedown analysis. Compared to the experimental fatigue testing, which allows the development of localized damage within the microstructure, the shakedown analysis is expected to result in a lower fatigue strength. Thus, it is in accordance with expectations that the numerical fatigue strength estimation remains conservative for the investigated feedmods.

4.4 Torque Arm Analysis

Using the estimated local yield and fatigue strength, the torque arm of a 3 MW research nacelle is optimized. Localized stresses are computed using an FE-model, developed for the model-based analysis of the force transmission in a rotor bearing support system [32], which has been extended to include the torque arm and the gearbox, shown in Fig. 18. Here, the torque arm geometry is highlighted in blue with available design spaces for shape optimization marked in red.

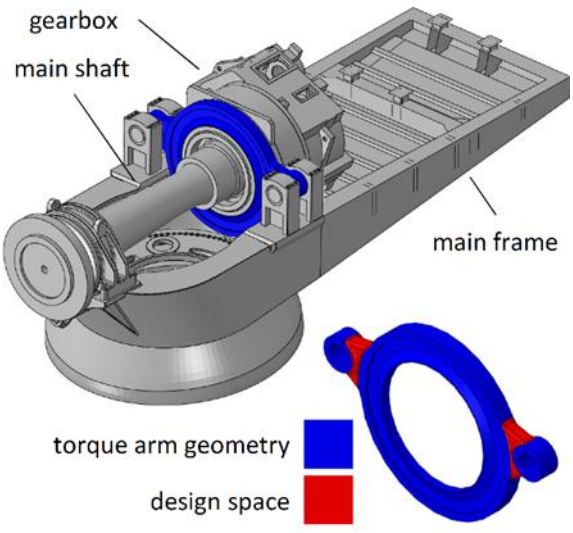


Fig. 18 Finite element model of the 3 MW research nacelle with the investigated torque arm.

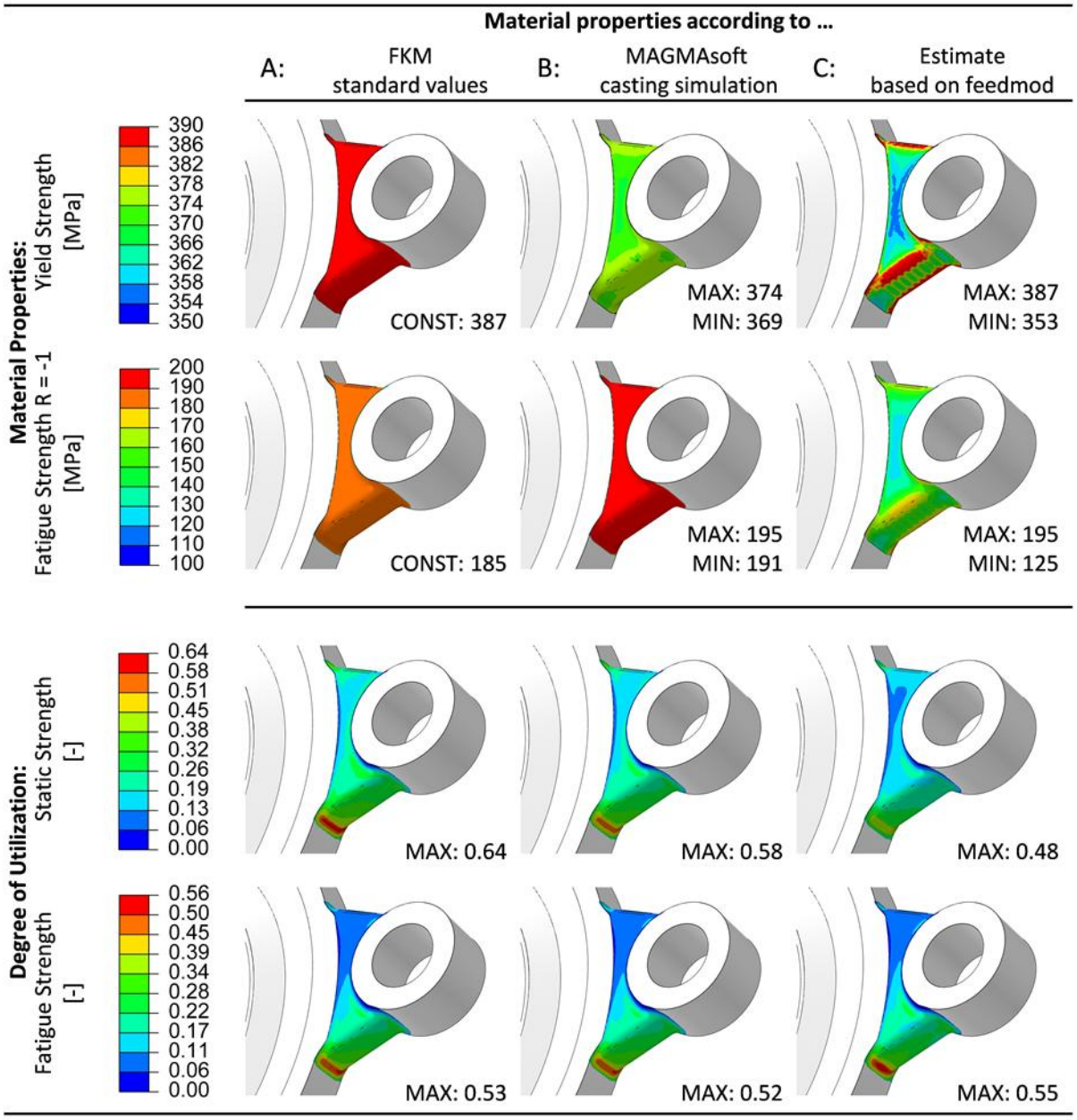


Fig. 19 Strength assessment results for different estimates of material properties.

Loadings are applied onto the main shaft of the FE model according to the IEC61400 guideline, which specifies operating conditions that must be considered during component design [33].

The critical region of the torque arm can be identified at the connection of the torque arm and the flange connection to the ring gear, as shown in the lower part in Fig. 19. The strength assessment at the identified critical region has been performed for the static and the fatigue strength using three sets of (local) predicted material properties: Set A consists of non-local parameters predicted according to FKM using the ultimate tensile strength obtained from uniaxial tensile tests. Set B considers localized material properties based on the locally computed ultimate tensile strength using MAGMAsoft casting simulation. Set C is based on feedmod dependent experimental yield strength and numerically estimated fatigue strength, later on referred to as estimated fatigue strength. The locally considered material properties for the different sets are presented in the upper part of Fig. 19. Here, FKM presents the highest estimation of the yield strength for the static strength assessment with a difference of 3.5 % compared to the MAGMAsoft based values. In order to

account for the validity ranges of experimental results, the maximum yield strength in set C is limited by the yield strength extrapolated to a feedmod of 1 cm. In contrast to the constant FKM yield strength value, the values according to MAGMAsoft have a local variance of 5 MPa, whereas consideration of experimental data results in a yield strength range of 34 MPa.

Larger differences can be observed for the fatigue strength. For set A (FKM) and set B (MAGMAsoft), the local fatigue strength is estimated using the ultimate tensile strength. In contrast to that, the local fatigue strength in set C is directly computed using the shakedown analysis under given microstructure descriptors obtained by the casting simulation. Here, a difference of up to 5.4% higher fatigue strength between MAGMAsoft and FKM can be observed. The maximum predicted fatigue strength (set C) of 195 MPa, which is the predefined saturation value, is only observed locally at the component edge and thus can be associated with numerical artifacts of the casting simulation. In the critical area, the numerically predicted fatigue strength is around 150 MPa, thus significantly lower than values according to FKM and MAGMAsoft. This is in accordance with estimations for two reasons: First, the shakedown analysis gives a conservative estimation of the fatigue strength by its concept. Second, the fatigue strength estimation based on the ultimate tensile strength is a purely empirical estimation such that it cannot account for localized defects, which are partially accounted for using the described cast iron specific safety factors.

The differences in local utilization for the static and fatigue strength assessment are presented at the bottom of Fig. 19. Here, utilization for the static strength assessment is performed under consideration of cast iron specific safety factor of 1.25. For both Magma based utilization and feedmod dependent yield strength, a reduced utilization of 9.4 % and 7.8 % can be observed, respectively. Thus, the presented feedmod dependent yield strength is in good agreement with Magma based results and results in component potential due to the reduced local utilization. For the fatigue strength assessment, the local utilization for set A and set B is computed under consideration of cast iron specific safety factor of 1.25. In contrast to that, the utilization of set C is computed without safety factors due to the conservative fatigue strength estimation by the shakedown theorem. Here, the local utilization is increased by 3.7 % for the estimated fatigue strength compared to FKM. The small difference may indicate here that the cast iron specific safety factors considered in FKM approach are inherently considered in local fatigue strength estimations using the presented approach. The overall good agreement of set C with set A and set B furthermore indicates that the presented consideration of safety factors is feasible. Considering the offset for experimental fatigue strength and shakedown analysis, shown in Fig. 17, the computed local fatigue strength utilization is affected. Thus, increased accuracy of the simulative prediction of the local fatigue strength will directly affect the local utilization. A reduction of the 10.4 % error in simulative strength prediction would result in a local utilization of 0.5. Compared to the fatigue strength utilization according to FKM a potential of 5.6 % can be identified. Therefore, while not resulting in an immediate component potential, the numerical estimation of local fatigue strength allows for a better understanding of local safety factors and a possible reduction of said safety factors as well as component optimization.

Ultimately, component optimization within the available design space of the torque arm can be achieved by reducing the opening angle of the torque arm during the shape optimization step. Reducing the opening angle and, thus, the load-bearing cross-section leads in turn to an increase in component stress and utilization in the critical region. Since the degree of utilization is defined as the ratio of component stress and component strength, the utilization increases proportionally to the component stress. Fig. 20 presents the local utilization in dependence of the opening angle under the assumption that required component stiffness and functionality are maintained. Here, the utilization according to FKM is considered in order to maintain a conservative shape optimization. An increase in local utilization can be seen with a decreasing opening angle. Therefore, allowance for a higher local utilization results in a weight reduction within the available design space of the torque arm. Since the utilization degree cannot exceed 1.0, the static strength assessment governs the torque arm design. If the utilization based on local material properties is considered instead of utilization according to FKM a further optimization of the torque arm can be expected as the governing static strength utilization is reduced.

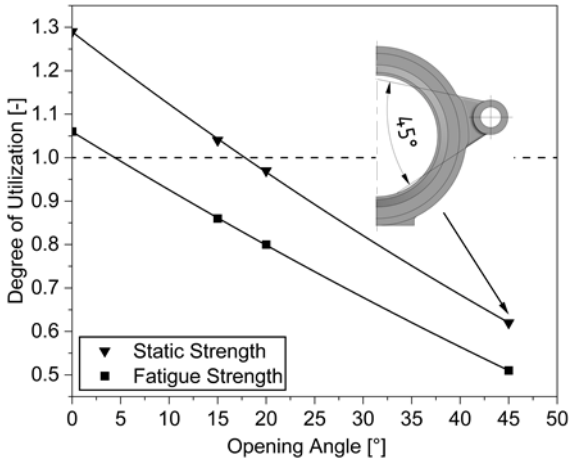


Fig. 20 Static and fatigue strength utilization in dependence of opening angle of the torque arm.

Fig. 21 presents the weight reduction in dependence of the opening angle. Here, the reduced opening angle leads to a weight reduction of up to 12.8 % or 212 kg with respect to the initial component weight. However, in this case, the overall weight reduction potential is limited by the maximum possible weight reduction for an opening angle of 0°.

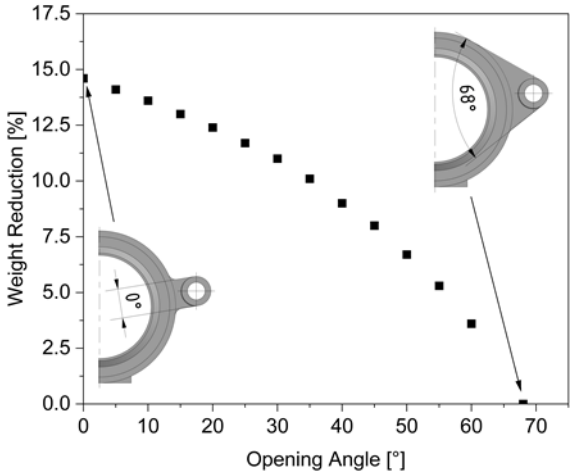


Fig. 21 Overall weight reduction of the torque arm in dependence of the opening angle.

Thus, it was shown that local material properties can be considered in the strength verification, and thus an additional potential for weight reduction can be achieved, which is in accordance with the results of [4].

5 Conclusion and Outlook

This study demonstrates the consideration of local material properties during the component design of heavy-section castings. Thereby, an improved understanding of the consideration of local material properties has been achieved. As a result of subsequent component optimization, a significant weight reduction could be achieved.

The fatigue behavior of heavy-section castings of ductile cast iron grade EN-GJS-500-14 has been characterized. Fracture surface analysis allowed for the identification of pores as the main crack initiation side. Combining the results of experimental material characterization and casting simulation leads to a correlation of local material properties with the results of the casting simulation. Using the obtained correlation, a functional description is derived, which allows the estimation of a local static material strength based on the cooling rate and particle count obtained by casting simulation. In order to estimate the local fatigue strength, the shakedown theorem has been applied and a feedmod dependent fatigue strength has been computed. A comparison of the estimated fatigue strength with experimental results suggests that the estimated fatigue strength is conservative, which is in accordance with the assumption of a damage-free material state made by the shakedown theorem. Thus, further component potential can be opened up if the accuracy of the numerical fatigue strength estimation is increased while maintaining conservativeness.

Using the derived feedmod dependent static and cyclic material properties, a local component strength is introduced into the FKM strength assessment. Using the estimated local component strengths, the torque arm of a 3 MW research nacelle has been optimized. From the definition of the degree of utilization, it can be seen that the utilization is inversely proportional to the material properties, such that a more accurate prediction of material properties can lead to a reduction of safety factors and thus increase the potential of the components. However, the degree of utilization is also proportionally related to the component stresses. Thus, the determination of the stresses must be further improved, e.g. by consideration of well-defined load collectives and more detailed component interactions, in parallel with the improved prediction of the material properties. In addition, extremely weight-optimized structural components must be examined during optimization with respect to function and influence on the system behavior since the component stiffness is changed due to design changes. The design process of cast iron components is consequently becoming increasingly interdisciplinary and requires more efficient methods, processes and toolchains. Nevertheless, a transfer of the proposed methods to other use cases is feasible and does not significantly com-

plicate the process of the strength assessment. However, material data and regressions need to be available for the desired use case and require experimental analysis. Especially deviations from the investigated material, for example due to changing manufacturing routes, may result in significant changes in local material properties and must be accounted for. Future work will continue to integrate local material properties into the strength assessment of heavy-section castings. Therefore, the scope of the presented correlation of material characterization and casting simulation needs to be validated by investigation of other ferritic cast iron grades. With respect to the estimation of the local fatigue strength, the shakedown approach is going to be extended by a criterion for allowance of limited localized damage. To ensure the applicability of local material properties in a strength assessment, the interaction of local material properties and required safety factors are going to be determined in the future.

6 Acknowledgments

This research has been funded by the Federal Ministry for Economic Affairs and Climate Action (BMWK) in the project LeKoGussWEA under grant number 0324279A.

Supported by:



on the basis of a decision
by the German Bundestag

7 References

[1] European Commission, The Commission calls for a climate neutral Europe by 2050, 2018.

[2] Bundesverband der Deutschen Gießerei-Industrie, Die Gießerei-Industrie. (2016).

[3] R. Rennert, E. Kullig, M. Vormwald, Analytical strength assessment of components Made of Steel, Cast Iron and Aluminium Materials in Mechanical Engineering: FKM Guideline, 7th ed., VDMA Verlag, Frankfurt/Main, 2020.

[4] R. Cenni, M. Cova, G. Bertuzzi, A methodology to consider local material properties in structural optimization, Proceedings of the Institution of Mechanical Engineers, Part C: Journal of Mechanical Engineering Science 231 (2017) 2822–2834.

[5] J. Olofsson, K. Salomonsson, I.L. Svensson, Modelling and simulations of ductile iron solidification- induced variations in mechanical behaviour on component and microstructural level, IOP Conf. Ser.: Mater. Sci. Eng. 84 (2015) 12026.

[6] J. Olofsson, K. Salomonsson, J. Johansson, K. Amouzgar, A methodology for microstructure-based structural optimization of cast and injection moulded parts using knowledge-based design automation, Advances in Engineering Software 109 (2017) 44–52.

[7] J. Olofsson, R. Cenni, M. Cova, G. Bertuzzi, K. Salomonsson, J. Johansson, Multidisciplinary shape optimization of ductile iron castings by considering local microstructure and material behaviour, Struct Multidisc Optim 57 (2018) 1889–1903.

[8] J. Dobrovska, J. Stettina, Two numerical models of the solidification structure of massive ductile castiron casting, Materials and technology 44 (2010) 93–98.

[9] C. Thomser, M. Bodenburg, J.C. Sturm, Optimized Durability Prediction of Cast Iron Based on Local Microstructure, Inter Metalcast 11 (2017) 207–215.

[10] J. Dobrovska, F. Kavicka, K. Stransky, B. Sekanina, J. Stetina, F. Barlat, Y.H. Moon et al., Numerical Optimization of the Method of Cooling of a Massive Casting of Ductile Cast-Iron, AIP Conference Proceedings 1252 (2010) 578–585.

[11] N. Bonora, A. Ruggiero, Micromechanical modeling of ductile cast iron incorporating damage. Part I: Ferritic ductile cast iron, International Journal of Solids and Structures 42 (2005) 1401–1424.

[12] T. Andriollo, J. Thorborg, J. Hattel, Modeling the elastic behavior of ductile cast iron including anisotropy in the graphite nodules, International Journal of Solids and Structures 100-101 (2016) 523–535.

[13] T. Andriollo, J. Thorborg, N.S. Tiedje, J. Hattel, Modeling of damage in ductile cast iron - The effect of including plasticity in the graphite nodules, IOP Conf. Ser.: Mater. Sci. Eng. 84 (2015) 12027.

[14] T. Andriollo, N. Tiedje, J. Hattel, Distance map based micromechanical analysis of the impact of matrix heterogeneities on the yield stress of nodular cast iron, Mechanics of Materials 148 (2020) 103414.

[15] C. Gebhardt, T. Sedlatschek, A. Bezold, C. Broeckmann, Full-field inverse identification of elasto-plastic model parameters for ductile cast iron, Mechanics of Materials 162 (2021) 104056.

[16] C. Gebhardt, G. Chen, A. Bezold, C. Broeckmann, Influence of graphite morphology on static

and cyclic strength of ferritic nodular cast iron, MATEC Web Conf. 165 (2018) 14014.
[17] C. Gebhardt, T. Trimborn, F. Weber, A. Bezold, C. Broeckmann, M. Herty, Simplified ResNet approach for data driven prediction of microstructure-fatigue relationship, Mechanics of Materials 151 (2020) 103625.
[18] P. Donelan, Modelling microstructural and mechanical properties of ferritic ductile cast iron, Materials Science and Technology 16 (2000) 261–269.
[19] DIN EN ISO 945-4:2016(E) working draft: microstructure of cast irons—part 4: test method for determining nodularity in spheroidal graphite cast irons.
[20] DIN 50125:2016-12, Prüfung metallischer Werkstoffe_- Zugproben, Berlin, Beuth Verlag GmbH, 10.31030/2577390.
[21] DIN 50100:1978-02, Schwingfestigkeitsversuch - Durchführung und Auswertung von zyklischen Versuchen mit konstanter Lastamplitude für metallische Werkstoffproben und Bauteile; Deutsche Fassung.
[22] M. Hempen, F. Klubberg, P. Beiss, PC-Software SAFD - statistical analysis of fatigue data (1998).
[23] D. Weichert, A. Hachemi, F. Schwabe, Shakedown Analysis of Composites, Mechanics Research Communications 26 (1999) 309–318.
[24] G. Chen, Strength Prediction of Particulate Reinforced Metal Matrix Composites, Shaker, Aachen, 2016.
[25] E. Melan, Zur Plastizität des räumlichen Kontinuums, Ingenieur-Archiv 9 (1938) 116–126.
[26] B. Widom, Random Sequential Addition of Hard Spheres to a Volume, The Journal of Chemical Physics 44 (1966) 3888–3894.
[27] P. Jelínek, T. Elbel, Chvorinov's rule and determination of coefficient of heat accumulation of moulds with non-quartz base sands, Archives of Foundry Engineering 10 (2010) 77–82.
[28] E. Foglio, M. Gelfi, A. Pola, D. Lusuardi, Effect of Shrinkage Porosity and Degenerated Graphite on Fatigue Crack Initiation in Ductile Cast Iron, Key Engineering Materials 754 (2017) 95–98.
[29] S. Borgs, W. Stets, Porosity in ductile cast iron and its influence on the mechanical performance under cyclic loading, Casting Plant & Technology 3 (2015) 8–21.
[30] J. Schindelin, I. Arganda-Carreras, E. Frise, V. Kaynig, M. Longair, T. Pietzsch, S. Preibisch et al., Fiji: an open-source platform for biological-image analysis, Nature methods 9 (2012) 676–682.
[31] T. Skaland, Ø. Grong, T. Grong, A Model for the Graphite Formation in Ductile Cast Iron: Part I. Inoculation Mechanisms, Metall Mater Trans A 24 (1993) 2321–2345.
[32] S. Reisch, G. Jacobs, D. Bosse, A. Loriemi, Experimental and Model-based Analysis of the Force Transmission in a Rotor Bearing Support System, J. Phys.: Conf. Ser. 1037 (2018) 62028.
[33] DIN German Institute for Standardization, Wind energy generation systems: Part 1: Design requirements, 61400th ed. 27.180(61400-1), Berlin, Beuth Verlag GmbH, 2019.